Journal of Organometallic Chemistry 695 (2010) 120–127

Contents lists available at ScienceDirect

Journal of Organometallic Chemistry

journal homepage: www.elsevier.com/locate/jorganchem

Periodic mesoporous silica-immobilized palladium(II) complex as an effective and reusable catalyst for water-medium carbon–carbon coupling reactions

Chunmei Kang, Jianlin Huang, Wenhan He, Fang Zhang *

Department of Chemistry, Shanghai Normal University, 100 Guilin Road, Shanghai 200234, China

ARTICLE INFO

Article history:
Received 14 August 2009
Received in revised form 14 September 2009
Accepted 25 September 2009
Available online 3 October 2009

Keywords:
Mesoporous organometallic catalyst
Evaporation-induced self-assembly
Water-medium organic reaction
Palladium
Carbon–carbon formation

ABSTRACT

Ethyl-bridged periodic mesoporous organosilicas (PMOs) functionalized with diphenylphosphino (PPh_2) ligands were synthesized by one-step evaporation-induced self-assembly (EISA), which were used as a support to immobilize Pd(II) organometallic catalyst by coordination reaction. The as-prepared Pd(II)–PPh_2–PMO(Et) exhibited high activity in water-medium C–C coupling reactions and could be used repetitively. The high activity could be attributed to the high dispersion of Pd(II) active sites and ordered mesopore channels which effectively diminished the steric hindrance and thus, diffusion limit. Meanwhile, the ethyl-fragments and the PPh_2-ligands in the support wall could synergic enhance surface hydrophobicity, which promoted the adsorption for organic reactant molecules.

1. Introduction

The creation of an economically and green chemical transformation represents a global grand challenge [1]. The use of water as a reaction medium to substitute organic solvents is considered as environmentally benign way due to it minimizes environmental impact, reduces the cost and presents smaller operational hazards [2,3]. Recently, the development of heterogeneous organometallic catalysts for water-medium organic reactions has provided a highly promising strategy with the attractions of ease of work-up, facile catalyst recovery and recycling and improved atom efficiency [4–10]. Grafting the organometallic complexes onto mesoporous silica materials by ligand-chelated route proved to be an appealing way to the heterogenization of homogeneous catalysts [11]. Thus, the amount and spatial arrangement of chelated ligands on the mesoporus silica is the critical factors that determine the existence state and distribution of active sites [12].

Periodic mesoporous organosilicas (PMOs) with organic groups bridged in the framework has been reported [13]. The feature of this material is that the organic groups are not located in the pores, but rather are an intrinsic part of the pore walls, which unique properties, such as hydrophobicity, could be designed to optimize the reaction micro-environment [14]. In general, introducing chelated organic moiety into PMOs could be achieved either by a grafting or co-condensation method in the hydrothermal condition [15]. Compared with grafting technique, the co-condensation method would likely result in PMOs with more uniform distribution of organic groups and higher loading of organic group without blocking the mesopores. However, this protocol is often difficult to keep various silanes with distinct hydrolyze rate match well, which incompatible process causes phase separation and further disrupt the mesostructure. The Evaporation Induced Self-Assembly (EISA) process provides the most promising routes for the synthesis of ordered mesoporous hybrid nanocomposites [16], because of some advantages over the hydrothermal synthesis such as controllable hydrolysis-condensation speed and easy integration with multiple building blocks [17,18]. Therefore, it would be of great interest to incorporate chelated ligands onto the PMOs by one-step EISA approach, which not only yield relatively uniform active sites with intact molecular structure to anchor organometallic catalysts, but can be integrated with PMOs specific properties to create favorable reaction environments [19].

In this present study, we reported our efforts to immobilize the Pd(II) organometallic catalyst in the ethane-bridged PMOs by EISA assembly and post-modification approach two-step combination method. This elaborated catalyst exhibited comparable catalytic activity and good selectivity with the corresponding homogeneous catalyst in the water-medium organic coupling reactions. Furthermore, this heterogeneous catalyst can be reused for at least six times with slight loss of catalytic activity.

* Corresponding author. Tel.: +86 21 64322642; fax: +86 21 64322272.
E-mail address: zhangfang@shnu.edu.cn (F. Zhang).

0022-328X/$ - see front matter © 2009 Elsevier B.V. All rights reserved.
doi:10.1016/j.jorganchem.2009.09.036

2. Experimental

2.1. Chemicals

The solvents are of analytical quality and dried by standard methods. Other materials are analytical grade and used as purchased without further purification. Triblock copolymer P123, dichlorobis(triphenylphosphine)palladium(II) and 1,2-bis(trimethoxysilyl)ethane (BTME) were purchased from Sigma–Aldrich Company Ltd. 2-(diphenylphosphino)ethyltriethoxysilane (DPPES) was obtained from Gelest Inc.

2.2. Synthetic procedures

2.2.1. Synthesis of PPh_2–PMO(Et)

In a typical synthesis, P123 (0.16 g) was dissolved in a solution containing HCl (0.023 ml, 0.50 M), ethanol (3.6 ml) and H_2O (0.25 ml) at 25 °C under vigorous stirring, followed by adding a solution containing 2.8 mmol 1,2-bis(trimethoxysilyl)ethane (BTME) and desired amount of 2-(diphenylphosphino)ethyltriethoxysilane (DPPES). Then, the solution was transferred into a Petri dish and the ethanol was evaporated at room temperature over 2 days. The solid product was scraped and crushed into powders, followed by refluxing in 500 ml ethanol for 24 h to extract surfactant and other organic residues. The as-received samples were denoted as PPh_2–PMO(Et)-*X*, where *X* is the molar percentage of DPPTS/(MBTMS+MDPPTS).

2.2.2. Synthesis of Pd(II)–PPh_2–PMO(Et)

About 0.20 g PPh_2–PMO(Et) was added into 6.0 ml toulene containing 0.10 g $PdCl_2(PPh_3)_2$. After being stirred for 12 h under argon atmosphere at 30 °C, the yellow powder product was filtered and washed thoroughly with freshly distilled toulene to eliminate uncoordinated Pd(II) complex, followed by vacuum drying at 60 °C, leading to Pd(II)–PPh_2–PMO(Et).

2.3. Characterization

The Pd content was determined by inductively coupled plasma optical emission spectrometer. Thermogravimetric analysis (TGA) was carried out on Shimadzu DTG-60 thermogravimetric analyzer with a ramping rate of 10 °C/min in 50 ml/min of air flow. Fourier transform infrared (FITR) spectra were recorded on a Thermo Nicolet Magna 550 spectrometer. Solid-state Nuclear magnetic resonance (NMR) spectra were obtained on a Bruker DRX-400 NMR spectrometer. X-ray powder diffraction (XRD) patterns were recorded on a Rigaku D/MAX B diffraction system with Cu Kα radiation. Transmission electron microscopy (TEM) morphologies were observed on a JEM-2011 at an acceleration voltage of 200 kV. Nitrogen sorption isotherms were measured at −96 °C on a Quantachrome NOVA 4000e system. The sample was degassed at 100 °C prior to the measurement. The specific surface area (S_{BET}), the pore size distribution curve, the pore volume (V_P) and the average pore diameter (D_P) were calculated by using the multiple-point Brunauer–Emmett–Teller (BET) method and the Barrett–Joyner–Halenda (BJH) model based on adsorption branches. The surface electronic states were analyzed by X-ray photoelectron spectroscopy (XPS, Perkin–Elmer PHI 5000C ESCA). All the binding energy values were calibrated by using C_{1S} = 284.6 eV as a reference.

2.4. Catalytic reactions

2.4.1. Water-medium Barbier reactions

Reaction A: Benzaldehyde (0.025 ml), allyl bromide (0.15 ml), $SnCl_2$ (0.45 g), 5.0 ml distilled water and a catalyst containing 0.050 mmol Pd(II) were mixed in a 10 ml three-necked round-bottomed flask. After reacting at 50 °C for 12 h under mild stirring, the products were extracted with toluene, followed by analysis on gas chromatograph (GC, Agilent 1790) equipped with a JWDB-5, 95% dimethyl 1-(5%)-diphenylpolysiloxane column and a FID detector. The N_2 is used as carrier gas and the column temperature is kept at 100 °C. The reproducibility is checked by repeating each result at least three times and is found to be within ±5%.

In order to determine the catalyst durability, the catalyst was allowed to settle down after each run of reactions and the clear supernatant liquid was decanted slowly. The residual solid catalyst was reused with fresh charge of water and reactant for subsequent recycle runs under same reaction conditions. The Pd content leached off from the heterogeneous catalyst was determined by ICP analysis.

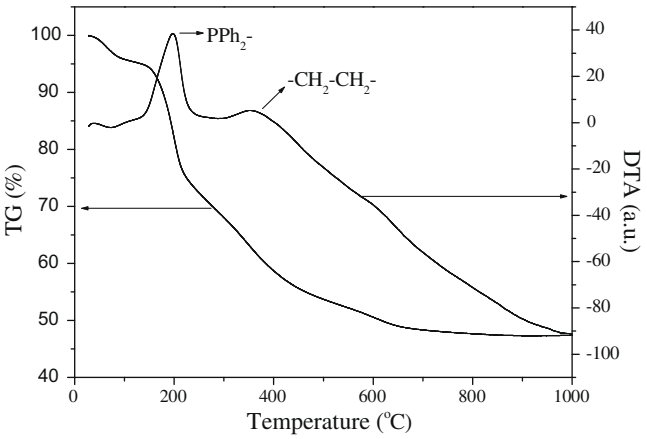

Fig. 1. TGA curves of the PPh_2–PMO(Et)-10 material.

2.4.2. Water-medium Sonogashira reactions

Reaction B: In each run of reactions, 0.025 g CuI, 1.0 g K_2CO_3, 0.050 g sodium lauryl sulfate, 2.5 ml distilled water, a catalyst containing 0.050 mmol Pd(II), 0.28 ml phenylacetylene and 0.58 ml benzoyl chloride were mixed and allowed to stir at 65 °C for 4 h. After extracted with toluene, the products were analyzed on a gas chromatograph as described in Barbier reactions.

Reaction C: 0.014 ml iodobenzene, 0.014 ml phenylacetylene, 0.21 ml DBU (1,8-diazabicyclo[5.4.0]undec-7-ene), 0.0050 g CuI,

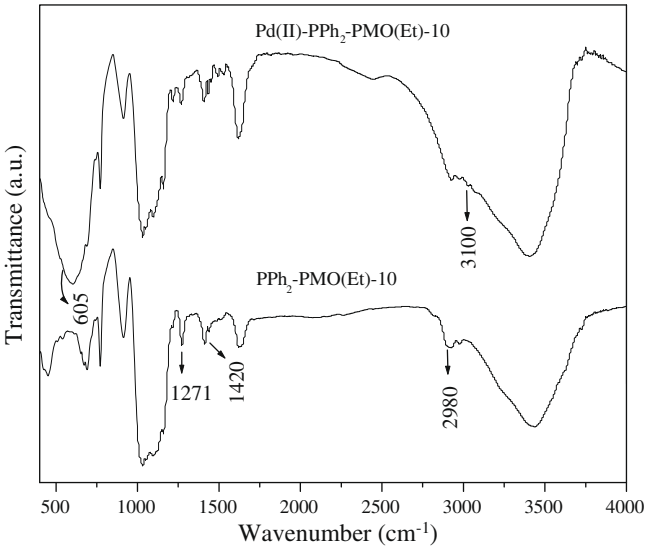

Fig. 2. FTIR spectra of the PPh_2–PMO(Et)-10 and Pd(II)–PPh_2–PMO(Et)-10 samples.

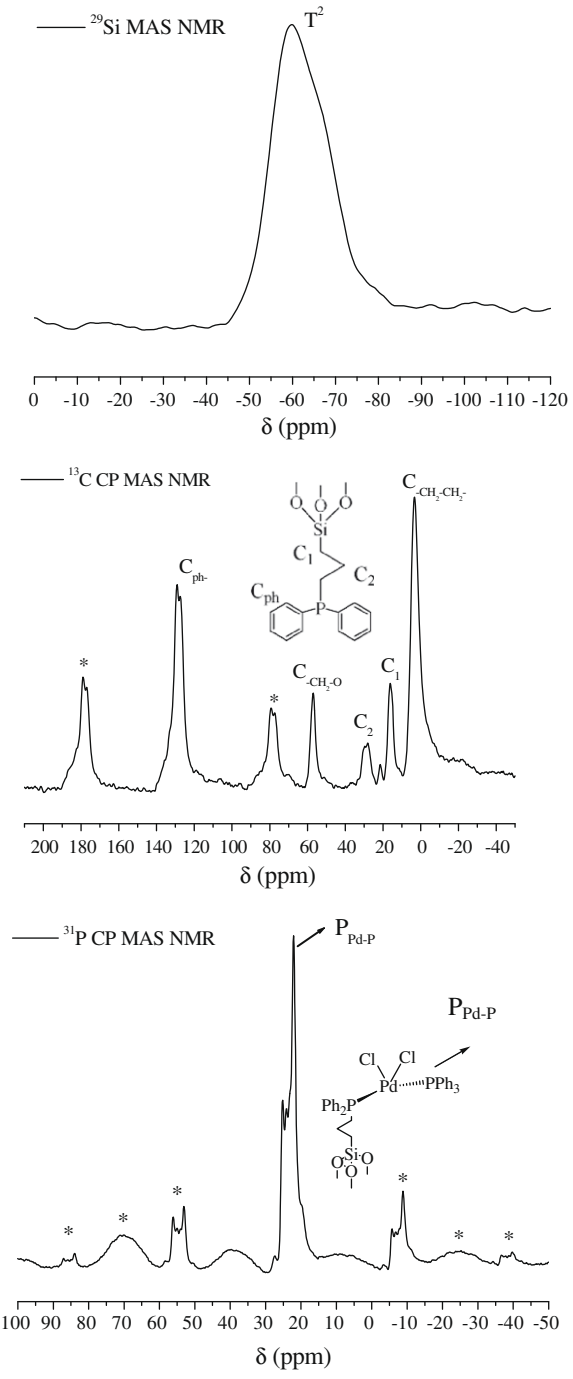

Fig. 3. Solid NMR spectra of the Pd(II)–PPh_2–PMO(Et)-10 catalyst.

4.0 ml distilled water and a catalyst containing 0.015 mmol Pd was allowed for stirring at 80 °C for 5 h. The products were extracted with toluene and analyzed on a gas chromatograph.

The selectivity of two coupling reactions could be determined by the external standard method from calibration curves with standard samples. The corresponding peak areas of the main-product and by-product ratio are calculated by GC apparatus, respectively. The selectivity is determined by the following equation:

$$\text{Selectivity}\,(\%) = \left[\frac{\text{Correct area of target product}}{(\text{Correct area of target product} + \text{Correct area of by-product})}\right] \times 100\%$$

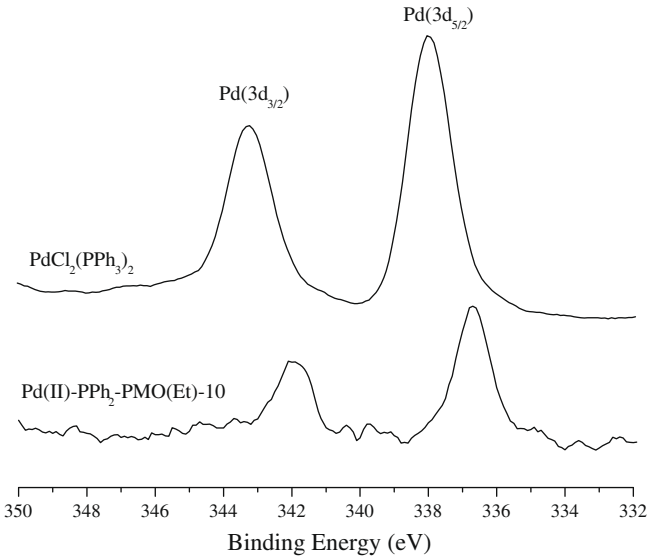

Fig. 4. XPS spectra of $PdCl_2(PPh_3)_2$ and Pd(II)–PPh_2–PMO(Et)-10 samples.

2.4.3. Investigation of Pd leaching

For the determination of the Pd content in solution a maximum amount of the clear filtrate was collected for precise Pd analysis (usually half of the reaction mixture). The defined amount of the clear filtrate was collected in a glass vessel immediately after hot filtration. After careful evaporation of the organic compounds, the sample was dissolved by aqua regia, diluted and the solution was filtered and the palladium content in solution was determined analyzed by inductively coupled plasma optical emission spectrometer (ICP-OES, Varian VISTA-MPX). The detection limit of our ICP apparatus for Palladium species is 0.05 ppm. Multiple analyses were applied for each sample for better accuracy.

3. Results and discussion

3.1. Compositional analysis

The PPh_2–PMO(Et) series samples, donated as PPh_2–PMO(Et)-*X* were prepared by the EISA assisted co-condensation between bis(trimethoxysilyl)ethane and (diphenylphosphino)ethyltriethoxysilane in which the loading of PPh_2 was adjusted by changing the molar percentage (X) of DPPTS/(MBTMS+MDPPTS). The Pd(II)–PPh_2–PMO(Et) samples were prepared by coordinating Pd(II) ions. The TGA curves (Fig. 1) demonstrated that the decomposition of organic groups in the extracted PPh_2–PMO(Et)-10 occurred between 180 and 450 °C, which showed weight loss of organic group about 25%. The first peak at 197 °C is attributed from the decomposition of the PPh_2-organic groups while the second peak at 352 °C comes from the decomposition of the bridged ethane moiety [20]. The FTIR spectra (Fig. 2) displayed three peaks at 1271, 1420 and 2980 cm^{-1}, corresponding to the C–H deformation vibration, the P–CH_2 vibration and the C–H stretching vibration, respectively. The P–PPh_2 vibration could not be distinguished from the intense Si–O bands. Compared to PPh_2–PMO(Et)-10 sample, the Pd(II)–PPh_2–PMO(Et)-10 revealed two additional absorbance peaks around 605 and 3100 cm^{-1} indicative of the δ_{C-H} and ν_{C-C} vibrations in the benzene ring connecting with the phosphorus (PPh_3-) [21]. The disappearance of the C–H bending vibration of P123 at 1377 cm^{-1} indicated almost complete removal of the surfactant using the EtOH extraction method. Combination of TGA and FTIR studies, it could be concluded that the PPh_2-ligands and Pd(II)

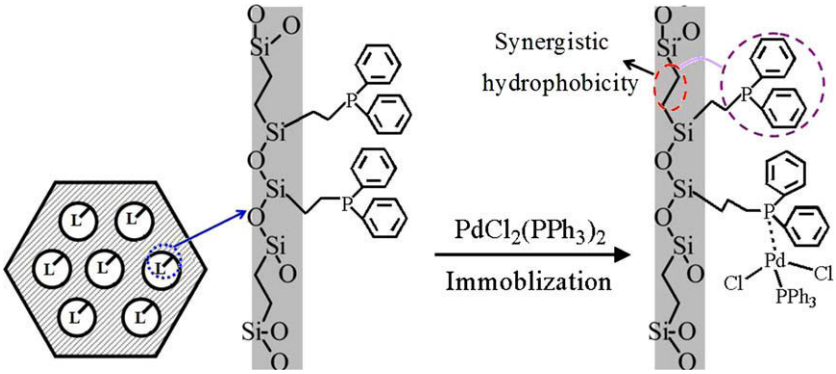

Scheme 1. Schematic diagram of the immobilization process for synthesizing Pd(II) periodic mesoporous organometallic catalysts.

complex were successfully anchored onto the PMOs support, which could be further confirmed by solid-state NMR spectra (Fig. 3). The ^{29}Si MAS NMR spectrum of Pd(II)–PPh_2–PMO(Et)-10 catalyst displayed an intense signal at −60.1 ppm, which demonstrated that only T^2 [$SiC(OH)(OSi)_2$] existed in the framework. The absence Q^n confirmed that the Si–C bond remains intact co-condensation.[20] The ^{13}C CP-MAS NMR spectrum displayed one sharp signal at 5.4 ppm was ascribed to the ethane moiety bridged in the mesoporous framework. Two peaks around 15 and 33 ppm, were attributed to the C atoms in the CH_2–CH_2 group connected to the phenylphosphine group and one peak around 138 ppm was indicative of the C atoms in the benzene ring in the phenylphosphine group. The peak at 58 ppm was probably attributed to the non-hydrolyzed ethoxide functionalities (CH_2–O), which could be corroborated by the major T^2 species in the ^{29}Si MAS NMR [22]. The ^{31}P CP-MAS NMR spectrum displayed an intense peak at 22 ppm indicative of the Pd–P bond [23], which further confirmed the existence of Pd(II) organometallic complex. Other peaks denoted by asterisks are the rotational sidebands, which often appeared in the CP-MAS high speed rotation process. The XPS spectra (Fig. 4) demonstrated that all the Pd species in the Pd(II)–PPh_2–PMO(Et)-10 presented in +2 oxidation state, corresponding to the binding energy (BE) of 337.4 eV in $Pd_{3d5/2}$ level [24]. In comparison with the BE of the Pd(II) in $Pd(PPh_3)_2Cl_2$, the BE of the Pd(II) in Pd(II)–PPh_2–PMO(Et)-10 shifted negatively by 1.3 eV (from 337.9 to 336.6 eV), indicating that the PPh_2-ligand could donate more electrons to Pd(II) than the PPh_3-ligand. These result further confirmed the immobilization of Pd(II) onto the PMOs support through coordinating with the PPh_2-ligand, as illustrated in Scheme 1.

3.2. Structural characterization

As shown in Fig. 5, the small-angle XRD patterns revealed that both the PPh_2–PMO(Et) and Pd(II)–PPh_2–PMO(Et) samples exhibited one intense peak indicative of (1 0 0) reflections, suggesting that the hexagonal arrayed pore structure (*p6mm*) observed could be preserved after modification with PPh_2-groups and even anchoring the Pd(II) organometallic catalyst. The d_{100} diffraction peak shifted to lower angle with the increasing organic moiety loading, suggesting the anchor of PPh_2-groups or Pd(II) complex onto the pore surface, leading to the enhanced thickness of pore walls (see Table 1) [20]. The decrease of the peak intensity implied that the PPh_2 modification and Pd(II) immobilization might disturb the ordered mesoporous structure to a certain degree. The TEM morphologies further confirmed that both the PPh_2–PMO(Et) and Pd(II)–PPh_2–PMO(Et) samples displayed a two-dimensional hexagonal arrangement of one-dimensional channels with uniform size, as shown in Fig. 6. Even after assembling with 15% organosilane

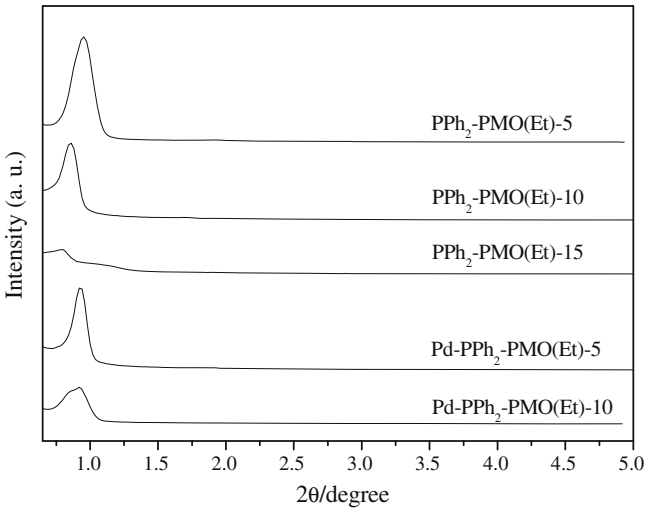

Fig. 5. XRD patterns of PPh_2–PMO(Et) and Pd(II)–PPh_2–PMO(Et) samples.

Table 1
Physicochemical parameters for PPh_2-functionalized periodic mesoporous materials and Pd(II) mesoporous organometallic catalysts.

Sample	a_0[a] (nm)	S_{BET} (m^2/g)	Pore volume[b] (cm^3/g)	Pore diameter[c] (nm)	Wall thickness[d] (nm)
PPh_2–PMO(Et)-5	11.1	533	0.50	4.5	6.6
PPh_2–PMO(Et)-10	11.8	523	0.59	5.8	6.0
PPh_2–PMO(Et)-15	12.7	348	0.54	6.4	6.3
Pd(II)–PPh_2–PMO(Et)-5	10.6	451	0.46	4.3	6.3
Pd(II)–PPh_2–PMO(Et)-10	11.5	341	0.39	5.3	6.2

[a] a_0 is the lattice parameter calculated from $a_0 = 2d_{100}/3^{1/2}$.
[b] Total pore volume was calculated at $P/P_0 = 0.99$.
[c] Analysis from adsorption isotherm.
[d] Wall thickness = a_0 − pore diameter.

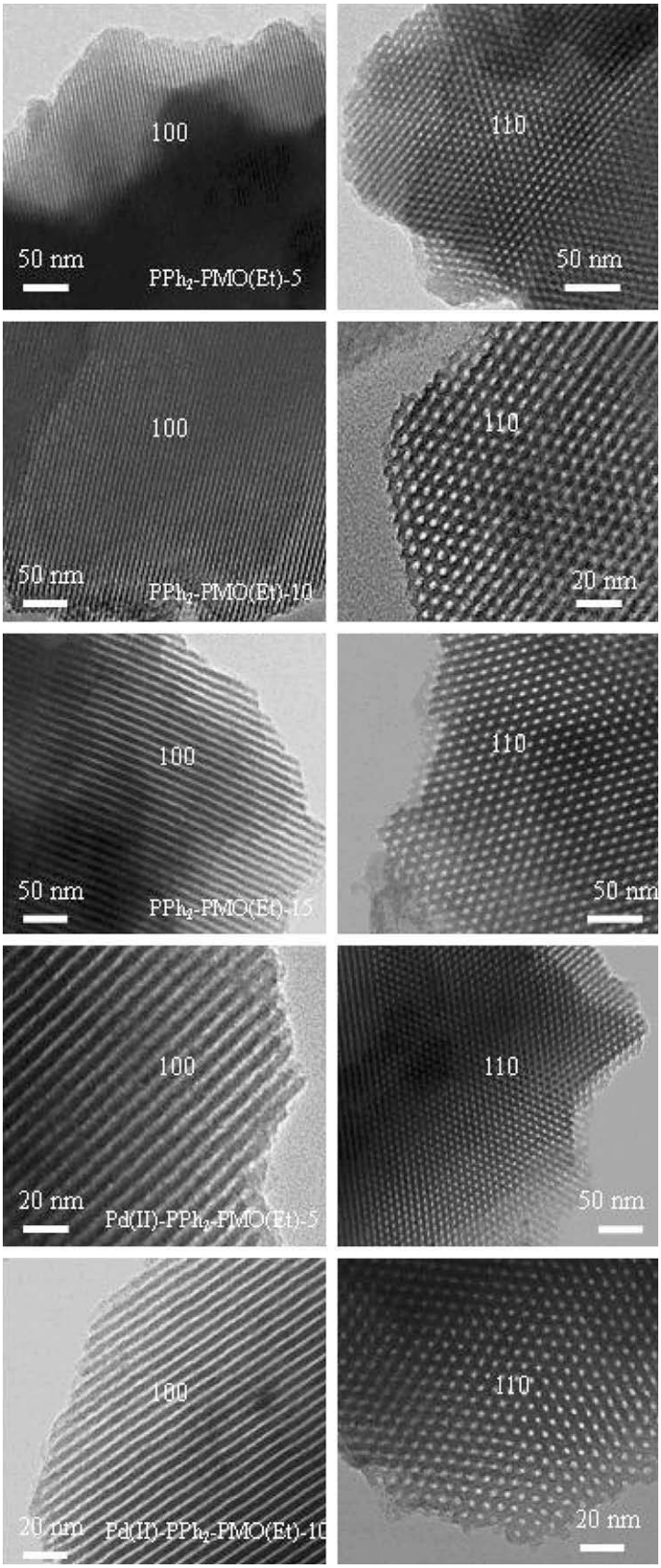

Fig. 6. TEM images of PPh_2–PMO(Et) and Pd(II)–PPh_2–PMO(Et) samples.

composed of chelated ligands, the mesoporous structure retained long-range ordering, which demonstrated EISA method could effectively assemble different silane building blocks to form high ordered mesostructure.

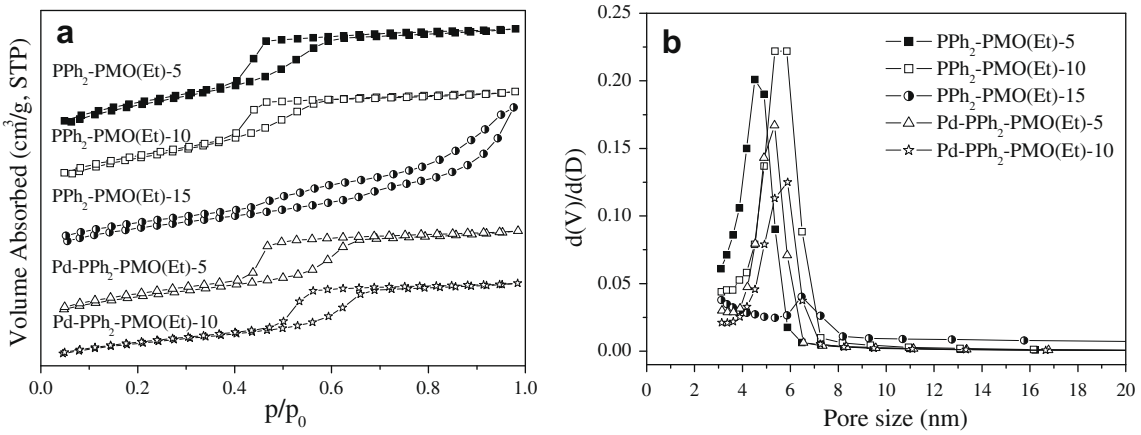

Fig. 7. N_2 sorption isotherms (a) and pore size distribution (b) of PPh_2–PMO(Et) and Pd(II)–PPh_2–PMO(Et) samples.

Table 2
Pd(II) catalyzed water-medium organic C–C coupling reactions.[a]

Reaction	Catalyst	Content (mmol)	Conversion (%)	Selectivity[b] (%)
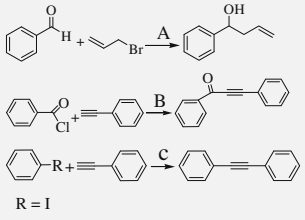	$PdCl_2(PPh_3)_2$	0.05	98.7	96.8
	Pd(II)–PPh_2–PMO(Et)-5	0.05	86.7	86.4
	Pd(II)–PPh_2–PMO(Et)-10	0.05	98.4	93.9
	$PdCl_2(PPh_3)_2$	0.05	97.1	96.7
	Pd(II)–PPh_2–PMO(Et)-5	0.05	84.6	95.0
	Pd(II)–PPh_2–PMO(Et)-10	0.05	95.2	95.5
	$PdCl_2(PPh_3)_2$	0.0145	99.9	98.9
	Pd(II)–PPh_2–PMO(Et)-5	0.0145	91.3	96.3
	Pd(II)–PPh_2–PMO(Et)-10	0.0145	99.9	99.1

[a] Detailed reaction conditions are described in the experimental section.
[b] The selectivity in the coupling reaction is determined by the external standard method in the gas chromatography apparatus.

Accordingly, all the PPh_2–PMO(Et) samples exhibited type IV nitrogen adsorption–desorption isotherms with H_1 hysteresis loop characteristic of mesoporous structure with the narrow range pore size distribution (Fig. 7). From Table 1, one could see that the pore size of the support increased with the PPh_2-content increasing, since the hydrolysis of DPPTS tends to insert into the area between hydrophilic and hydrophobic groups of surfactant, serving as a swelling agent to enlarge the pore channels [25]. Immobilization with Pd(II) organometallic complex resulted in the decrease of S_{BET}, D_P and V_P due to partial damage of the mesoporous structure. Compared to PPh_2–PMO(Et) materials, the decrease of the unit cell parameters and the broad distribution of pore size in the Pd(II)–PPh_2–PMO(Et) evidenced that the organometallic complexes in the grafted mesoporous samples are mainly located on internal surfaces of the mesoporous materials.

Table 3
Screening of different substance in the water-medium Sonogashira reactions.[a]

Entry	R–	Catalyst	Conversion (%)	Selectivity[b] (%)
1	CH_3O–	$PdCl_2(PPh_3)_2$	99.9	99.9
		Pd(II)–PPh_2–PMO(Et)-10	99.9	99.6
2	CH_3–	$PdCl_2(PPh_3)_2$	99.9	98.5
		Pd(II)–PPh_2–PMO(Et)-10	99.9	98.3
3	NO_2–	$PdCl_2(PPh_3)_2$	99.9	98.6
		Pd(II)–PPh_2–PMO(Et)-10	99.9	97.8

[a] Reactions were carried out at 80 °C in 4.0 ml H_2O using 0.02 mmol iodobenzene, 0.02 mmol substituted phenylacetylene compound and 0.0145 mmol Pd(II) catalyst.
[b] The selectivity in the Sonogashira reaction is determined by the external standard method.

3.3. Catalytic properties of mesoporous organometallic catalysts for water-medium clean organic reactions

Palladium-catalyzed carbon–carbon cross-coupling reactions are some of the most important processes in synthetic organic chemistry [26]. To investigate the utility of our novel Pd(II) periodic mesoporous organometallic catalysts, the water-medium coupling reactions involved with aryl aldehyde, alkenes, and alkynes are car-

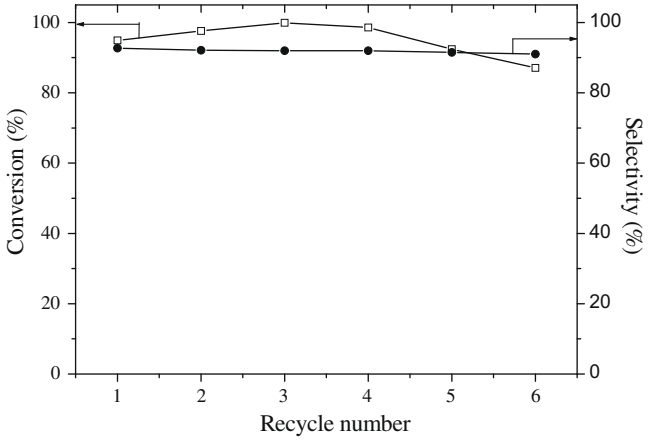

Fig. 8. Recycle test of Pd(II)–PPh_2–PMO(Et)-10 catalyst in the water-medium Barbier reaction.

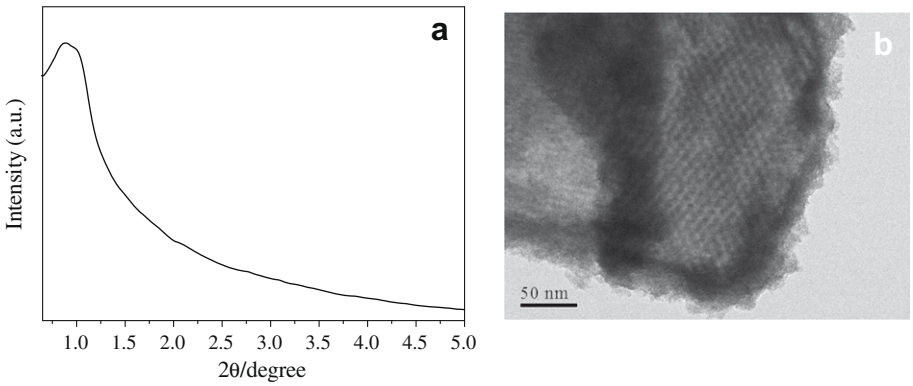

Fig. 9. XRD spectrum (a) and TEM image (b) of Pd(II)–PPh_2–PMO(Et)-10 after reused for 6 times.

ried out under the procedure described in the experimental section (Table 2). Table 2 summarized the catalytic performance of different catalysts with the same absolute Pd(II) content in each reaction system. The Pd(II)–PPh_2–PMO(Et)-10 catalyst exhibited higher conversion and selectivity than the Pd(II)–PPh_2–PMO(Et)-5 since the latter has the lower density of active sites, which reduce the possibility of the contact between the substance and the active sites. More interesting, the Pd(II)–PPh_2–PMO(Et)-10 catalyst showed similar catalytic performance as $PdCl_2(PPh_3)_2$ homogeneous catalyst in all three coupling reactions. It seemed reasonable to conclude that the excellent catalytic performance should be attributed to the high dispersion of Pd(II) active sites which provided high accessibility of the reactants to the actives sites and enhanced surface hydrophobicity derived from both bridged ethyl groups and the PPh_2-ligands which promoted the diffusion and adsorption of organic molecules [27]. Moreover, we tested this Pd(II) mesoporous catalyst with various substances in the water-medium Sonogashira reaction (Table 3). As expected, a series of functional groups on the phenyl ring of iodobenzene, such as methyl, methoxy and nitro, were compatible under this procedure, and yields for these reaction are generally equal to that of homogenous catalyst.

To make sure whether the heterogeneous Pd(II) complex on the PPh_2–PMO(Et) support or the dissolved homogeneous Pd(II) complex was the real catalytic species, the following procedure, proposed by Sheldon et al. was carried out [28]. After reaction for 6 h that the conversion exceeded 45% in Barbier reactions, the mixture was filtered to remove the solid catalyst and then allowed the mother liquor to react for another 20 h under the same reaction conditions. No significant activity was observed, demonstrating that the active species were not the dissolved Pd(II) complexes leached from Pd(II)–PPh_2–PMO(Et)-10. Therefore, it was reasonable to suggest that the present catalysis is heterogeneous in nature.

Fig. 8 showed the durability of the Pd(II)–PPh_2–PMO(Et)-10 catalyst during water-medium Barbier reaction. No significant decrease in the selectivity was observed after being used repetitively for 6 times. However, the conversion and thus the yield decreased slightly with the increase in repetitive times. To investigate the specific reasons for the decline in activity, we firstly employed the ICP analysis to evaluate the leaching degree of Pd(II)–PPh_2–PMO(Et)-10. ICP analysis demonstrated that, after being used for 5 recycles, the content of Pd(II) species in the solution was less than 10 ppm, showing that the loss of the active Pd(II) sites could be neglected. However, both the XRD spectrum and the TEM image (Fig. 9) demonstrate that ordered mesoporous structure has been partially destroyed after being used six times. Accordingly, the damage of the ordered mesoporous structure was perhaps the main reason responsible for the deactivation of the Pd(II)–PPh_2–PMO(Et)-10 catalyst.

4. Conclusion

In summary, we develop a general approach to synthesize highly dispersed organometallic complex supported on PMOs materials using EISA assembly method associated with immobilization. The EISA method provides an effective way to prepared functionalized PMOs with high loading anchoring sites. The post-grafting of $PdCl_2(PPh_3)_2$ on the PPh_2-modified PMOs generates novel mesoporous organometallic catalysts (Pd(II)–PPh_2–PMO(Et)). This heterogeneous catalyst showed high activity and stability in the water-medium organic coupling reactions, presumably a result of favorable hydrophobic micro-environment and the ordered mesoporous structure. The combinatorial assembly route is of great potential in the controlled synthesis of high active PMOs-supported organometallic catalysts for various chemical transformations.

Acknowledgements

This work was supported by the National Natural Science Foundation of China (20825724), Chinese Education Committee (20070270001), the Special Doctorial Project (20070270001), Shanghai Government (07dz22303) and Leading Academic Discipline Project of SHNU (DZL807).

References

[1] P.T. Anastas, M.M. Kirchhoff, Acc. Chem. Res. 35 (2002) 686–694.
[2] C.J. Li, Chem. Rev. 93 (1993) 2023–2035.
[3] C.J. Li, Chem. Rev. 105 (2005) 3095–3166.
[4] S. Minakata, M. Komatsu, Chem. Rev. 109 (2009) 711–724.
[5] H.X. Li, H. Yin, F. Zhang, H. Li, Y.N. Huo, Y.F. Lu, Environ. Sci. Technol. 43 (2009) 188–194.
[6] F. Zhang, G.H. Liu, W.H. He, Y. Hong, X.S. Yang, H. Li, J. Zhu, H.X. Li, Y.F. Lu, Adv. Funct. Mater. 18 (2008) 3590–3597.
[7] H.X. Li, M.W. Xiong, F. Zhang, J.L. Huang, W. Chai, J. Phys. Chem. C 112 (2008) 6366–6371.
[8] G.H. Liu, M. Yao, F. Zhang, Y. Gao, H.X. Li, Chem. Commun. (2008) 347–349.
[9] H.X. Li, F. Zhang, Y. Wan, Y.F. Lu, Green Chem. 9 (2007) 500–505.
[10] K.R. Jain, F.E. Kuhn, J. Organomet. Chem. 692 (2007) 5532–5540.
[11] C. Li, Catal. Rev. 46 (2004) 419–492.
[12] D.E. De Vos, I.F.J. Vankelecom, P.A. Jabobs, Chiral Catalyst Immobilization and Recycling, Wiley-VCH, Weinheim, Germany, 2000.
[13] S. Ingagaki, S. Guan, Y. Fulushima, T. Ohsuna, O. Terasaki, J. Am. Chem. Soc. 121 (1999) 9611–9614.
[14] Q.H. Yang, J. Liu, L. Zhang, C. Li, J. Mater. Chem. 19 (2009) 1945–1955.
[15] F. Hoffmann, M. Cornelius, J. Morell, M. Froba, Angew. Chem. Int. Ed. 45 (2006) 3216–3251.
[16] C.J. Brinker, Y.F. Lu, A. Sellinger, H.Y. Fan, Adv. Mater. 11 (1999) 579–585.
[17] E.L. Crepaldi, G.J. Soler-Illia, D. Grosso, F. Cagnol, F. Ribot, C. Sanchez, J. Am. Chem. Soc. 125 (2003) 9770–9786.
[18] S.C. Warren, U. Wiesner, Pure Appl. Chem. 81 (2009) 73–84.
[19] K. Andreas, D. Markus, K. Ralf, A. Heinz, B. Thomas, Chem. Eur. J. 15 (2009) 6645–6650.

[20] D.M. Jiang, J.S. Gao, Q.H. Yang, J. Yang, C. Li, Chem. Mater. 18 (2006) 6012–6018.
[21] Q.Y. Hu, J.E. Hampsey, N. Jiang, C.J. Li, Y.F. Lu, Chem. Mater. 17 (2005) 1561–1569.
[22] J.J. Yang, I.M. EI-NahhaI, I.S. Chuang, G.E. Maciel, J. Non-Cryst. Solids 212 (1997) 281–291.
[23] J.H. Nelson, J.A. Rahn, W.H. Bearden, Inorg. Chem. 26 (1987) 2192–2193.
[24] B.M. Choudary, K.R. Kumar, Z. Jarnil, G. Thyagarajan, Chem. Commun. (1985) 931–932.
[25] Y.D. Xia, R. Mokaya, J. Phys. Chem. B 107 (2003) 6954–6960.
[26] K.C. Nicolaou, P.G. Bulger, D. Sarlah, Angew. Chem. Int. Ed. 44 (2005) 4442–4489.
[27] Y. Wan, D.Q. Zhang, Y.P. Zhai, C.M. Feng, J. Chen, H.X. Li, Chem. Asia J. 2 (2007) 875–881.
[28] R.A. Sheldon, M.I. Wallau, W.C.E. Arends, U. Schuchardt, Acc. Chem. Res. 31 (1998) 485–493.